Fragment emission in the interaction of ^{238}U with 400 GeV protons

D. L. Klingensmith and N. T. Porile
Department of Chemistry, Purdue University, West Lafayette, Indiana 47907
(Received 11 February 1988)

Differential ranges at five angles to the beam have been measured for 23 fragments, ranging from ^{47}Ca to ^{143}Ce, produced in the interaction of ^{238}U with 400 GeV protons. Energy spectra obtained from the data show evidence for the presence of two components, which can be attributed to deep spallation and to fragmentation or fission. The spectra have been compared with a thermal model, used to test the two-step model of high-energy reactions, subjected to an invariant cross section analysis, and compared with the predictions of the Hüfner fast breakup model.

I. INTRODUCTION

The measurement of recoil properties of radioactive products is one of the techniques that has been used for the elucidation of nuclear reaction mechanisms. Depending on the type of target-catcher configuration used, recoil experiments can yield the mean kinetic energies of reaction products, the mean longitudinal momentum transferred in the interaction, the angular distribution of the products, and the double-differential cross sections for the formation of specific products. This last type of experiment, which involves differential range measurements covering a set of narrow angular intervals, yields the most detailed information obtainable from recoil measurements. The experiment is equivalent to an inclusive measurement of the energy spectra of charge- and mass-identified products performed over a broad angular range. It has the additional advantage of permitting measurements to be extended to energies well below the low-energy cutoff of counter experiments. Thus the energy regime below the peak in the spectra can be explored in detail.

The first measurement of differential ranges of high-energy proton reaction products emitted at specific angles to the beam was performed by Cumming *et al.*[1] These workers measured the differential ranges of ^{24}Na fragments emitted at three angles to the beam in the interaction of bismuth with 2.9 GeV protons. The data were used to examine the symmetry of the angular distribution in a system moving with a velocity determined from the kinematic shift in the spectra. A number of additional studies of this type have been reported.[2–5] Poskanzer and collaborators[6,7] have performed similar studies by direct measurement of energy spectra. The results of these various experiments indicate that, depending on the identity of target and product as well as on the incident proton energy, the angular distributions in the moving system can be either forward peaked, backward peaked, or symmetric about 90°. These experiments show that the two-step model of high-energy reactions applies to some reactions in certain proton energy regimes but not to others.

In addition to using their data to test the two-step model, Fortney and Porile[5] examined the angular distribution of scandium fragments produced in the interaction of uranium with 400 GeV protons as a function of their kinetic energy. They found that the highest-energy fragments were preferentially emitted at forward angles in the laboratory system while the lowest-energy fragments were preferentially emitted at backward angles. These angular distributions were based on measurements at only three angles and therefore were of limited significance. Nonetheless, Hüfner and Sommermann[8] were able to give a qualitative explanation of the results in terms of a fast breakup model.

The present work involves a more detailed study of the type performed by Fortney and Porile,[5] involving, in addition, a much wider range of products. We report the differential ranges at five angles to the beam for 23 products of the interaction of ^{238}U with 400 GeV protons. In addition to permitting a test of the two-step model, the results can be recast in the form of angular distributions as a function of product energy. Furthermore, the data have been obtained at sufficient angles to permit an invariant cross section analysis. Such an analysis provides information concerning the source of the observed products.

In a previous paper[9] we have reported the results of differential range measurements on products from the interaction of ^{238}U with 400 GeV protons performed at 90° to the beam. This paper should be consulted concerning the general experimental procedure as well as background information about the mechanisms believed to be of importance in the formation of specific products.

II. EXPERIMENTAL

The irradiations were performed with 400 GeV protons in an evacuated chamber located in an external beam line at Fermilab. The targets consisted of thin (0.2–0.3 mg/cm^2) UF_4 deposits evaporated over a 1×1 cm^2 area onto 25 μm thick, 99.999% pure aluminum foil.

Two types of experiments were performed. The differential ranges were measured at five angles covering the intervals of 10°–30°, 45°–65°, 80°–100°, 115°–135°, and 150°–170°. Fragments emitted at these angles were stopped in a stack of thin ($\sim$0.3 mg/cm^2) Mylar foils. These foils were mounted in cylindrical geometry at a

distance of 9.2 cm from the target. The solid angles subtended by the catchers were nearly constant, ranging from 0.37 sr at the most forward or backward angles to 0.33 sr at 90°. The targets were oriented at 90° to the beam in experiments designed to measure the differential ranges at 20° or 160°, and at 45° or 135° to the beam in those designed for measurements at the other angles.

The angular distributions were measured in a separate set of experiments. High-purity (99.999%) aluminum catcher foils, 15 mg/cm^2 in thickness, i.e., sufficiently thick to stop all recoils, were used to collect fragments emitted at the same angular intervals as in the differential range experiments. Two targets were placed back to back at 45° and 135° to the beam so that the entire angular distribution could be determined in a single experiment. The aluminum foils separating the two targets were sufficiently thick to prevent any cross contamination of recoils. The angular interval of 80°–100° was measured for both targets, thereby permitting a normalization of the forward and backward halves of the angular distribution. In turn, the angular distributions were used to normalize to each other the differential ranges of a given product emitted at the various angles.

The angular distribution and each differential range were measured three times. The irradiations had a duration of approximately one week. Following irradiation, the various foils were transported to Purdue University and assayed with calibrated Ge(Li) detectors. Owing to the large number of samples and to their relatively low activities, each foil could be assayed only once or twice. The results obtained from the γ-ray spectra are therefore limited to γ rays with either a clean one-component decay curve or with a two-component decay curve in which the longer-lived component contributed less than 5% of the activity throughout the entire assay time of approximately four days. The decay curves of these γ rays as well as the nuclidic assignments were determined in a separate experiment.[9]

The γ-ray spectra were analyzed with the code SAMPO,[10] and the differential ranges and angular distributions were obtained from the data as described elsewhere.[9,11–13] The differential ranges were corrected for the obliqueness of the paths followed by the recoils traversing the catchers, for the finite thickness of the catcher foils and the resulting loss in resolution, and for energy loss and broadening in the UF_4 targets. The corrections have been described in detail in another publication.[9] The average magnitudes of these corrections were approximately 5%, 7%, and 8%, respectively.

The corrected differential ranges were transformed to energy spectra by means of a code[14] that used the range-energy tables of Northcliffe and Schilling[15] as input. A 3–10 % correction was applied to account for the difference between the tabulated[15] path lengths and the experimentally determined projected ranges. The magnitude of this correction was based on the work of Lindhard *et al.*[16] as developed by Cumming.[17] Since the range-energy relation depends on product Z, the actual Z values were corrected for isobaric feedin as described elsewhere.[9] The energy spectra were converted to absolute differential cross sections on the basis of measured[18–25] or estimated[26] production cross sections for the nuclides of interest.

III. RESULTS

The energy spectra of some typical products, ^{48}Sc, ^{72}As, and ^{96}Nb, are displayed in Figs. 1–3, respectively. The average uncertainty in the data points is 11%, and is chiefly comprised of the uncertainties in the γ-ray intensity measurements (7%), the corrections to the differential ranges (4%), and the range-energy relation (7%).

As discussed in our previous report,[9] ^{48}Sc is typical of fragments with $A < 50$ in displaying a spectrum with a single broad peak at moderately low energies. The spectrum of ^{72}As is typical of both intermediate mass fragments ($A \sim 60$–80) and of neutron-deficient products in the fission product mass region. The spectra of these products are characterized by the presence of two com-

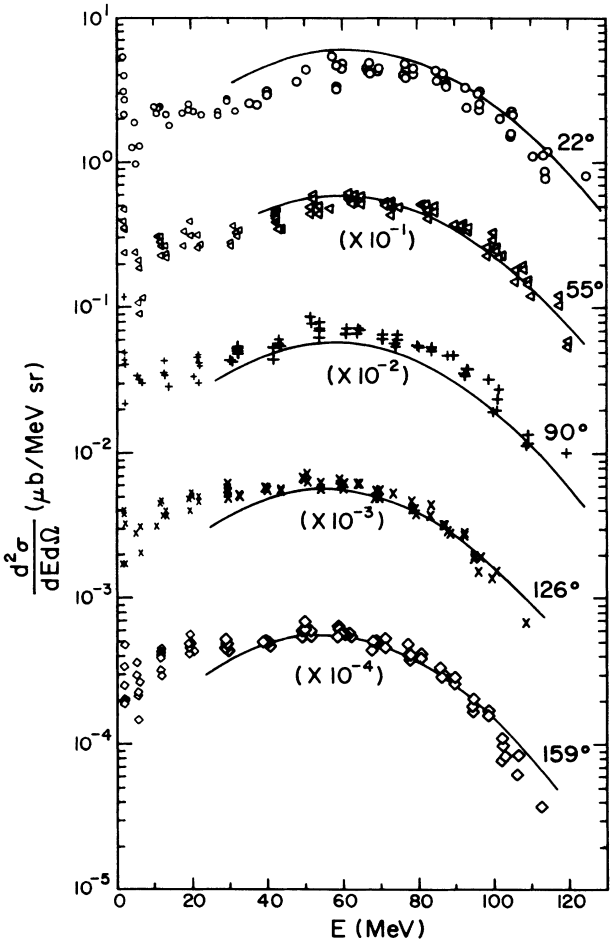

FIG. 1. Laboratory energy spectra of ^{48}Sc produced in the interaction of ^{238}U with 400 GeV protons. The solid curves give the results of a thermal model fit to all the data points represented by the large symbols. The low-energy data (small symbols) were not included in this fit.

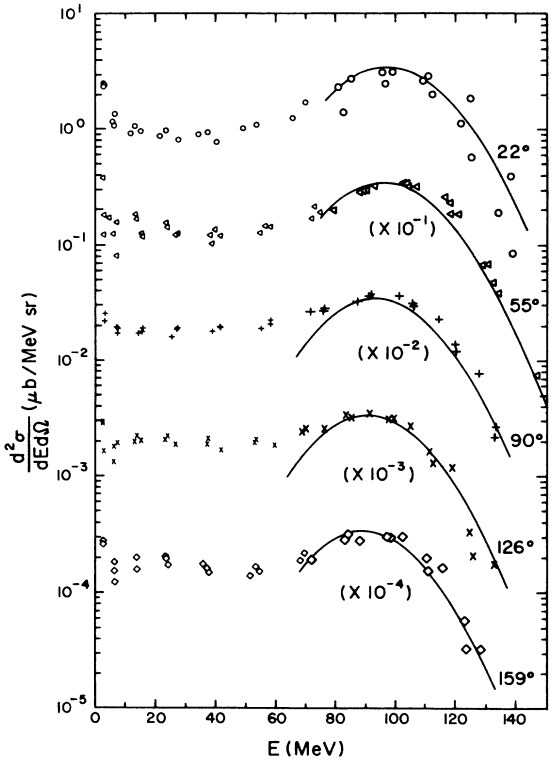

FIG. 2. Laboratory energy spectra of ^{72}As produced in the interaction of ^{238}U with 400 GeV protons. See Fig. 1 for details.

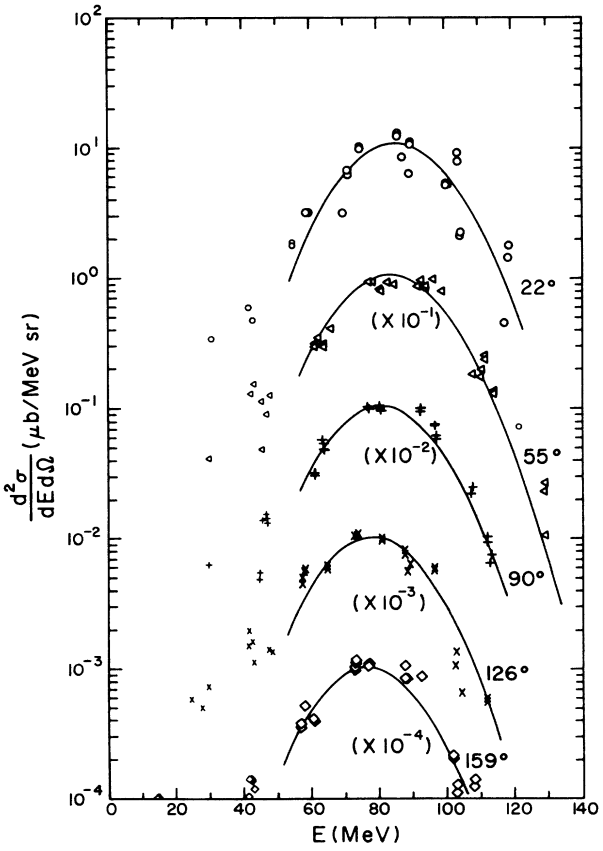

FIG. 3. Laboratory energy spectra of ^{96}Nb produced in the interaction of ^{238}U with 400 GeV protons. See Fig. 1 for details.

ponents present in nearly comparable amounts. The high-energy component has a Maxwellian-like shape, similar to that of fission products, while the low-energy component increases in yield with decreasing energy, as expected for deep spallation. Finally, ^{96}Nb has a spectrum characteristic of a fission product, with a single dominant component peaking at relatively high energies.

Figures 4 and 5 show some typical angular distributions. The error bars on the data points are based primarily on the uncertainties in the SAMPO fits. The points are plotted at the mean angle corresponding to each interval. The differential cross sections were normalized to unity at 90°. The solid curves represent least-squares fits to the data of the function

$$F(\theta_{\rm lab})=1+A_1\cos\theta_{\rm lab}+A_2\cos^2\theta_{\rm lab}\ . \qquad (1)$$

Table I summarizes the values of A_1 and A_2 for all the products of interest. The various products have been divided into the same two groups as in our previous work[9] on the basis of whether their energy spectra show the

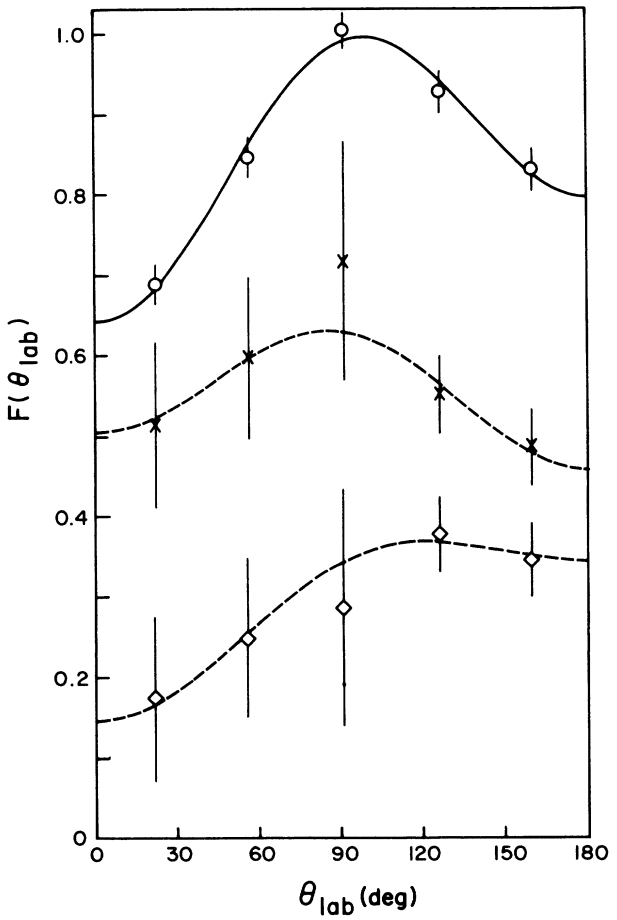

FIG. 4. Angular distribution of ^{72}As. The solid curve represents a fit of Eq. (1) to the data. The points labeled × and ◇ represent the relative contribution of the high- and low-energy mechanisms, respectively, to the experimental data (○). The dashed curves represent scaled fits of Eq. (1) to the data.

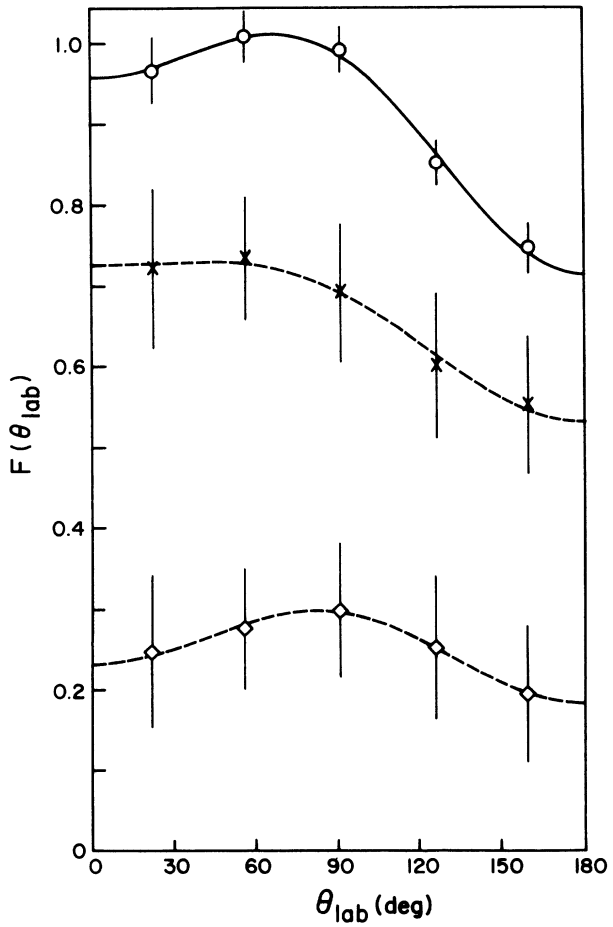

FIG. 5. Angular distribution of ^{120}Sb^{m}. See Fig. 4 for details.

presence of one or two components. The angular distributions shown in Figs. 4 and 5, which are for nuclides with two components, have been decomposed into curves for the individual components as discussed in the following section.

The angular distributions resemble closely those reported in a previous study of the interaction of ^{238}U with 400 GeV protons.[27] All the curves show a distinct peak at sideward angles. In some instances the differential cross sections at the most forward angles are larger than those at the corresponding backward angles ($A_1 > 0$) and in others the opposite holds true ($A_1 < 0$).

IV. DISCUSSION

A. Thermal breakup model fit

The presence of a peak in the spectra at Coulomb-like energies suggests that the high-energy component can be fit with a model which assumes that a moving remnant with temperature T breaks up into two or more fragments. The mechanisms responsible for this component are presumably fragmentation in the case of the light products ($A \leq 70$) and fission.[9] Numerous fits of this general type have been reported.[6,7,9,11,28] Our particular parametrization incorporates a Gaussian distribution of Coulomb energies B, with a most probable energy B_0 and a standard deviation σ, and two-body kinematics to correct for recoil:

TABLE I. Angular distribution and velocity parameters of products from the interaction of ^{238}U with 400 GeV protons.

Product	A_1	A_2	$10^3\beta$	$\langle\eta\rangle_R$	$\langle\eta\rangle_\theta$
		One-component spectra			
^{47}Ca	−0.028±0.043	−0.389±0.081	1.57±0.16	0.034±0.002	0.009±0.020
^{48}Sc	−0.087±0.017	−0.314±0.030	1.53±0.07	0.032±0.001	−0.021±0.008
^{82}Br	0.028±0.026	−0.251±0.056	1.27±0.03	0.030±0.001	0.016±0.012
^{95}Zr	−0.076±0.033	−0.144±0.067	0.67±0.06	0.015±0.001	−0.044±0.016
^{96}Nb	−0.008±0.024	−0.048±0.041	1.22±0.03	0.029±0.001	−0.008±0.012
^{97}Zr	−0.011±0.015	−0.154±0.028	0.73±0.02	0.016±0.000	−0.005±0.008
^{99}Mo	0.056±0.013	−0.203±0.024	0.70±0.03	0.017±0.000	0.024±0.006
^{105}Rh	0.003±0.019	−0.117±0.036	0.63±0.04	0.016±0.000	0.005±0.010
^{115}Cd	−0.016±0.019	−0.082±0.037	0.72±0.03	0.019±0.000	−0.008±0.010
^{127}Sb	−0.068±0.021	−0.377±0.042	0.57±0.03	0.016±0.000	−0.024±0.011
^{132}Cs	0.011±0.017	−0.310±0.032	0.69±0.00	0.019±0.000	0.001±0.009
^{140}Ba	−0.034±0.022	−0.268±0.041	0.33±0.02	0.010±0.000	−0.001±0.010
^{143}Ce	0.021±0.029	−0.197±0.057	0.38±0.03	0.012±0.000	0.016±0.014
		Two-component spectra			
^{67}Cu	0.032±0.020	−0.194±0.042	1.57±0.08	0.038±0.001	0.025±0.010
^{69}Zn^{m}	−0.036±0.033	−0.167±0.051	1.64±0.10	0.039±0.001	−0.001±0.016
^{72}Ga	−0.079±0.016	−0.258±0.031	1.24±0.07	0.030±0.001	−0.041±0.008
^{72}As	−0.078±0.016	−0.274±0.031	1.25±0.08	0.029±0.001	−0.040±0.008
^{76}As	−0.014±0.023	−0.294±0.046	1.46±0.04	0.037±0.001	0.000±0.012
^{96}Tc	−0.064±0.013	−0.345±0.024	1.20±0.05	0.036±0.001	−0.044±0.007
^{101}Rh^{m}	−0.019±0.015	−0.247±0.030	0.72±0.07	0.024±0.001	−0.011±0.008
^{103}Pd	−0.003±0.020	−0.151±0.037	0.71±0.04	0.019±0.001	0.002±0.010
^{120}Sb^{m}	0.124±0.022	−0.153±0.041	1.21±0.02	0.041±0.001	0.068±0.011
^{124}I	0.024±0.024	−0.141±0.045	0.86±0.04	0.028±0.001	−0.017±0.012

$$\frac{d^2\sigma}{dE_{\rm lab}d\Omega}=N\left[\frac{E_{\rm lab}}{E_{\rm c.m.}}\right]^{1/2}\int_0^{\min(E_{\rm c.m.},\rm BTS)}(E_{\rm c.m.}-B)^{1/2}\exp\left[\frac{-(B-B_0)^2}{2\sigma^2}\right]\exp\left[\frac{-\nu(E_{\rm c.m.}-B)}{T}\right]dB\ . \quad (2)$$

The energy of a fragment in the moving system $E_{\rm c.m.}$ is related to the laboratory energy $E_{\rm lab}$ by the expression

$$E_{\rm c.m.}=E_{\rm lab}+E_0-2(E_{\rm lab}E_0)^{1/2}\cos\theta_{\rm lab}\ , \quad (3)$$

where $E_0=\frac{1}{2}A_F v^2$, and A_F is the fragment mass. The factor $\nu=A_R/(A_R-A_F)$ provides for recoil correction, where the assumed mass of the remnant of the initial proton-nucleus interaction is $A_R=220$. The quantity BTS is the usual tangent-spheres barrier, and N provides the overall normalization.

The velocity v of the moving system can be decomposed into components directed along and perpendicular to the beam direction, designated $v_\parallel$ and $v_\perp$, respectively. The results of the fit are insensitive to the magnitude of $v_\perp$. A relatively large value of $v_\perp$, i.e., $v_\perp \gtrsim v_\parallel$, leads to a broader spectrum at 90° than at forward or backward angles. In addition, the mean energy in the moving system should be larger at 90° than at the other angles.[1,2] Since these effects were not observed, we conclude that $v_\perp < v_\parallel$ and approximate v by $v_\parallel$.

Equation (2) was used to perform a simultaneous least-squares fit to all the spectra of a given product using the code MINUIT.[29] This procedure assumes that the angular distribution is isotropic in the moving system. The solid curves in Figs. 1–3 are the results of this fit. The agreement between the curves and the data is typical of all the observed products. While small discrepancies are not readily apparent because of the compressed scale, some of the curves visibly tend to underfit the 90° spectra, as would be expected from the sideward peaking of the angular distributions.

The values of $\beta=v/c$ are listed in Table I and plotted versus product mass in Fig. 6. The underfitting of the 90° spectra does not affect the values of β. The β values exhibit an approximate inverse dependence on mass number and range from about 3×10^{-4} to 2×10^{-3}. The scatter in the β values indicates that the uncertainties may be larger than those given by MINUIT. There does not appear to be a significant difference between the one- and two-component products.

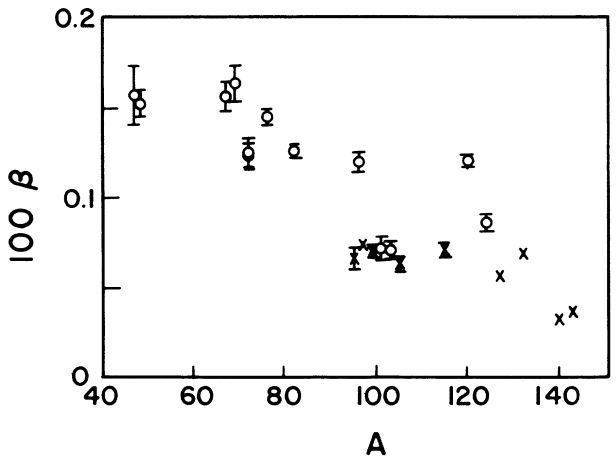

FIG. 6. Mass dependence of β values obtained from thermal model fit. ×, neutron-excessive fission products; ○, other products.

A previous study[7] of the energy spectra of F-Ar fragments formed in the interaction of ^{238}U with 4.9 GeV protons gave $\beta=6\times10^{-3}$, i.e., three to four times larger than the β derived from the lightest fragments observed in the present study. A decrease in β with increasing proton energy above ~3 GeV has been inferred previously from the change in angular distributions from forward peaked to sideward peaked[12] as well as from the decrease with energy of the forward-backward ratios obtained in thick-target recoil studies.[20,30] However, these conclusions depend on the applicability of the two-step model whereas the results derived from the kinematic shift in the spectra are independent of the validity of this model.

The very low values of β obtained at high energies, even in interactions in which substantial excitation energy must be transferred to the remnant, can be understood in terms of the results of Nakai *et al.*[31] These workers observed that a central high-energy proton-nucleus collision involves the forward emission of a moving source consisting of nucleons and mesons. This moving source carries off most of the energy and virtually all of the momentum of the incident proton. Consequently the excited remnant is formed with practically no longitudinal momentum.

The values of the other parameters determined from the fit of Eq. (2) are close to those derived previously from the fits to the 90° spectra.[9] As discussed in this earlier work, the values of B_0, expressed as a fraction of the tangent spheres value, are approximately 0.8 for neutron-excessive fission products, 0.6 for neutron-deficient fission products and intermediate mass fragments, and 0.3 for the lightest fragments. The standard deviations of the barrier distribution as well as the temperatures are significantly smaller for the neutron-excessive fission products than for the other products. These results are consistent with the fact that the formation of neutron-excessive fission products requires much lower excitation energies than that of the other products.

The low-energy component in the spectra of neutron-deficient fission products and intermediate mass fragments has been attributed to deep spallation.[9] The relative contributions of this component were obtained by subtraction of the Maxwellian fits from the measured spectra. Figure 7 shows the variation with angle of the percent contribution of the deep spallation component for typical products. In all instances, the contribution increases with angle by some 10–25% over the angular range of interest. The angular distributions of the deep

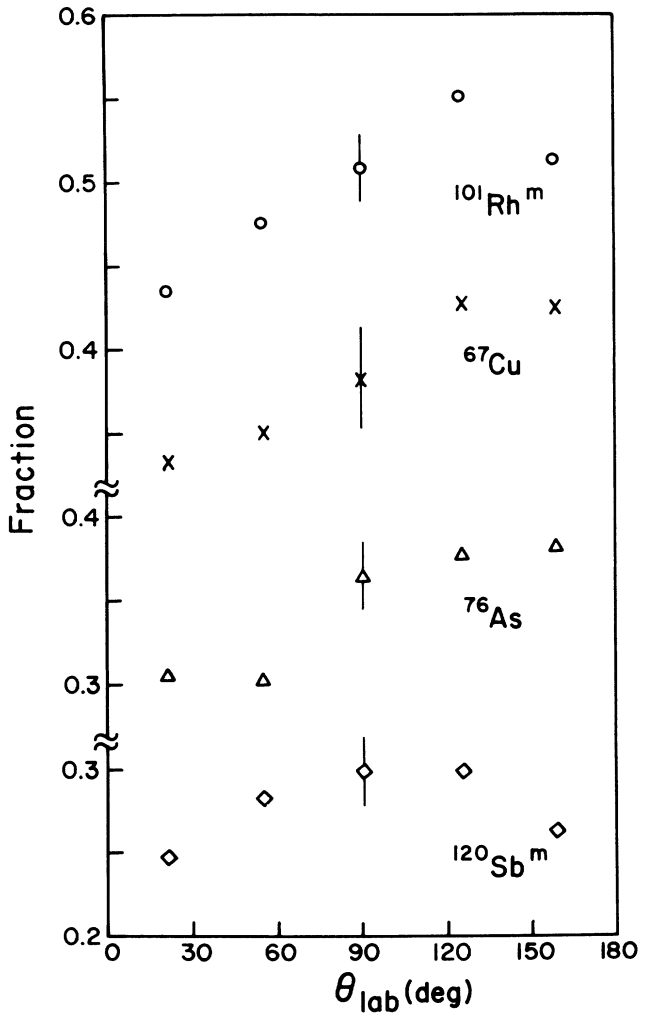

FIG. 7. Angular dependence of the fractional contribution of deep spallation to the energy spectra of various fragments.

spallation component consequently are enhanced at backward angles relative to the overall angular distributions, as illustrated in Figs. 4 and 5.

B. Two-step model analysis

The energy spectra and angular distributions may be used to test the applicability of the two-step vector model to the reactions of interest. According to this commonly used model of high-energy reactions, the laboratory velocity $\mathbf{v}_L$ of a particular product is expressed as the vector sum of two velocities, $\mathbf{v}_L = \mathbf{v} + \mathbf{V}$. The velocity $\mathbf{v}$ is that acquired by the remnant as a result of the initial proton-nucleus interaction and, in the simplest version of the model, is assumed to be directed along the beam. The velocity $\mathbf{V}$ is that acquired by the fragment in the breakup step. Since the two-step model assumes a temporal separation between the impact and breakup steps, the angular distribution of $\mathbf{V}$ in the moving system must, on average, be symmetric about the beam direction, but can be anisotropic.

The angular distributions yield values of $\langle \eta \rangle_\theta = \langle v/V \rangle$. This velocity ratio determines the transformation of the angular distribution from the laboratory system to the moving system and can be determined from a standard two-parameter fit to the angular distribution.[12] The second parameter in this fit is the anisotropy coefficient, which is numerically equal to A_2 in Eq. (1). The energy spectra yield the values of $\langle \eta \rangle_R = \langle v \rangle / \langle V \rangle$. The values of $\langle v \rangle$, i.e., β, were derived from the kinematic shift in the spectra by means of Eq. (2), as discussed in the preceding section. The values of $\langle V \rangle$ were obtained by means of the relation

$$\langle V \rangle^2 = \langle v_L \rangle^2 + \langle v \rangle^2 - 2\langle v_L \rangle \langle v \rangle \cos\theta_{lab} \tag{4}$$

which follows directly from Eq. (3). In turn, the values of $\langle v_L \rangle$ were obtained by transforming the differential ranges to velocity spectra and averaging over all the spectra obtained for a given product.

The values of $\langle \eta \rangle_\theta$ and $\langle \eta \rangle_R$ are tabulated in Table I. Provided that the slight difference in averaging as well as the effect of correlations between v and V are neglected, the two-step model demands that these two ratios have the same value for a given product, i.e., that the angular distribution in a system moving with a velocity obtained from the kinematic shift in the spectra by symmetric about 90°. Figure 8 shows the mass dependence of $\langle \eta \rangle_\theta$ and $\langle \eta \rangle_R$. It is seen that for most products the values of $\langle \eta \rangle_R$ are significantly larger than those of $\langle \eta \rangle_\theta$, which are actually negative for many nuclides. While this discrepancy could already be inferred from a careful examination of the fit of Eq. (2) to the spectra of a given product, the comparison of the two sets of $\langle \eta \rangle$ values makes the disagreement more readily apparent. While a positive correlation between v and V will lead to

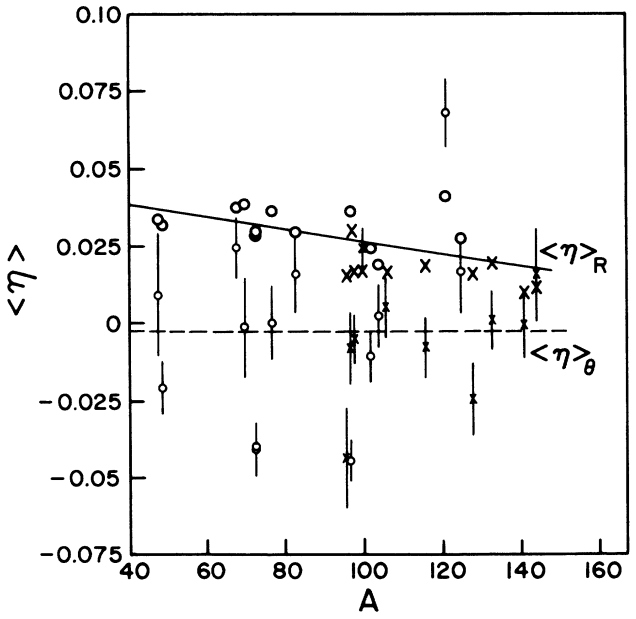

FIG. 8. Mass dependence of $\langle \eta \rangle_R$ and $\langle \eta \rangle_\theta$. Large symbols $\langle \eta \rangle_R$; small symbols $\langle \eta \rangle_\theta$. ×, neutron-excessive fission products; ○, other products. The lines show the trends in the data.

$\langle\eta\rangle_\theta < \langle\eta\rangle_R$,[1,2] correlations cannot lead to $\langle\eta\rangle_\theta$ and $\langle\eta\rangle_R$ of opposite signs. We therefore conclude that the formation of most products is inconsistent with the two-step model. As shown in Fig. 8, this conclusion applies to intermediate mass fragments as well as to some of the neutron-deficient and neutron-excessive fission products. A similar analysis has been performed for just the high-energy component in the spectra. Qualitatively similar results are obtained, albeit with larger uncertainties.

C. Invariant cross-section analysis

An informative presentation of inclusive data is in terms of a contour plot of the invariant cross sections,[32] $(1/p)(d^2\sigma/dEd\Omega)$. The abscissa in this plot is the rapidity and the ordinate is $p_\perp/mc$. For the nonrelativistic fragments of present interest, these quantities reduce to the parallel and perpendicular components of the fragment velocity expressed in units of c, $\beta_\parallel$, and $\beta_\perp$, respectively. Contour plots of constant invariant cross section are a useful tool in the analysis of reactions that may involve more than one mechanism since they give an indication of the motion of the sources of the observed fragments.

Some typical contour plots are shown in Fig. 9. The curves are two-parameter least-squares fits to the data points and consist of semicircles centered on the rapidity axis.[33] The parameters of the fit are the source velocity along the beam direction β_s, which defines the center of the semicircle, and the radial velocity β_r, which corresponds to its radius. Since we believe that the low-energy fragments generally are formed in a different process than the energetic fragments, we distinguish between them by means of dashed (low-energy) and solid contours. The curves provide a reasonably good fit to the data. The one systematic discrepancy is that, with the exception of the fission products, many of the curves underestimate the value of β_r at 90°. This discrepancy can be eliminated by moving the center of the semicircles off the β_s axis, i.e., by adding a transverse component to the motion of the emitting source, β_t. Figure 10 shows the resulting three-parameter fits to the data.

The values of the source velocity β_s are marked on the contour plots in Figs. 9 and 10. A distinct difference in the variation of β_s with β_r is observed for the high- and low-energy components. Thus the source velocities ob-

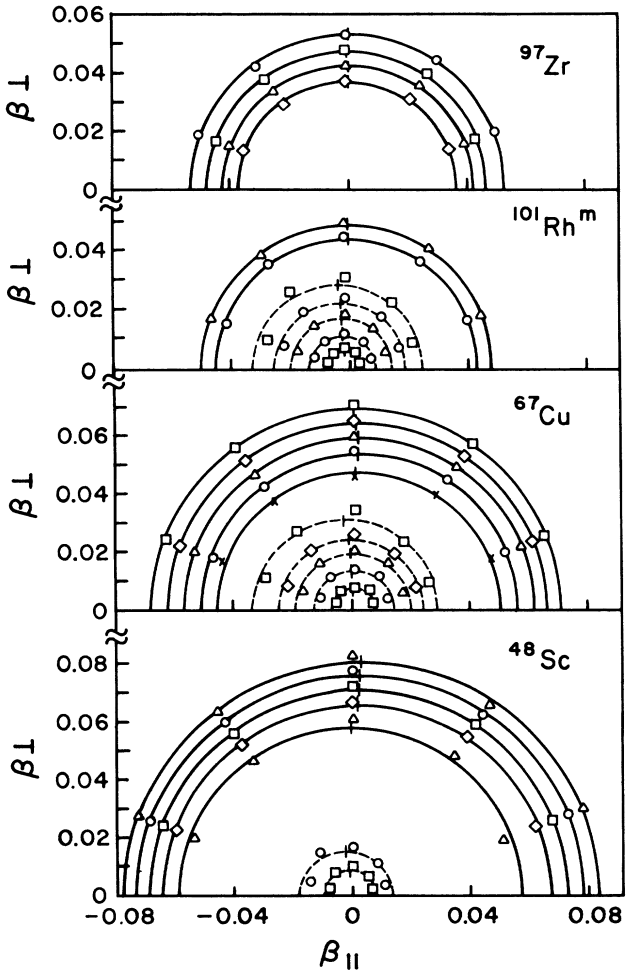

FIG. 9. Constant invariant cross sections for light fragments (^{48}Sc), intermediate-mass fragments (^{67}Cu), neutron-deficient fission products (^{101}Rh^m), and neutron-excessive fission products (^{97}Zr). The curves represent semicircle fits to the data points. The dashed and solid curves are drawn through points lying in the deep spallation and fission and/or fragmentation regions of the spectra, respectively. Adjacent dashed contours correspond to a factor of 2 change in invariant cross section; adjacent solid contours correspond to a factor of 10 change in invariant cross section. The values of β_s are given by the short vertical lines.

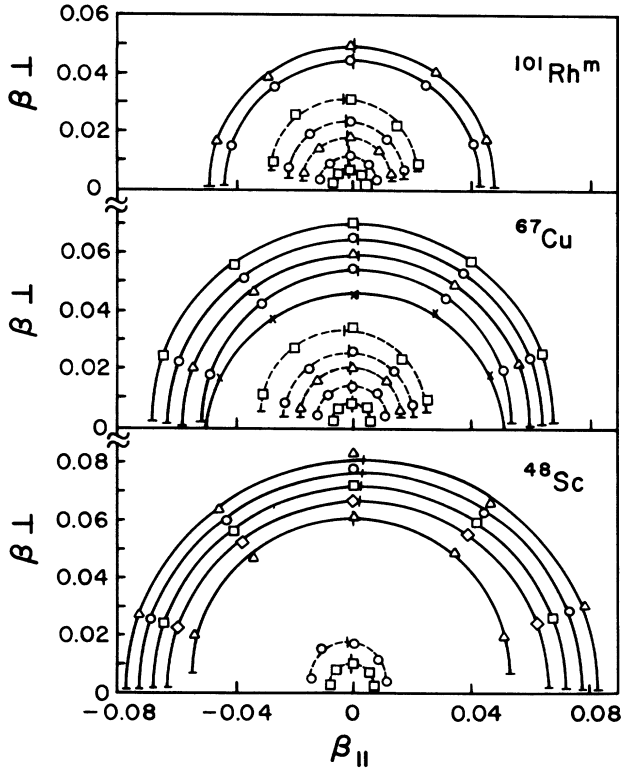

FIG. 10. Three-parameter fits $(\beta_s,\beta_t,\beta_r)$ to the invariant cross section points in Fig. 9.

tained from the contours associated with fission or fragmentation generally have small positive values and show no systematic variation with β_r. On the other hand, the source velocities associated with the deep spallation component tend to be negative, and become increasingly negative with increasing β_r. The values of β_t correspond to the vertical displacements of the semicircles off the β_s axis in Fig. 10. It can be seen that the values of β_t increase with β_r for the contours associated with the low-energy process. In contrast, β_t appears to be independent of β_r for the high-energy process.

The results for all the observed products can be summarized in plots of the mass dependence of the mean values of β_s and β_t. Separate averages for the high- and low-energy components are shown in Figs. 11 and 12, respectively. The variation of β_s and β_t with β_r can be summarized for each product by the values of $d\beta_s/d\beta_r$ or $d\beta_t/d\beta_r$ for each mechanism, as obtained from a linear fit. The mass dependence of these slopes is shown in Figs. 13 and 14 for the high- and low-energy components, respectively. Finally, Fig. 15 shows the mass dependence of $d\beta_t/d\beta_s$, the slope of the straight-line fit to the values of β_t and β_s associated with each contour for the deep spallation component.

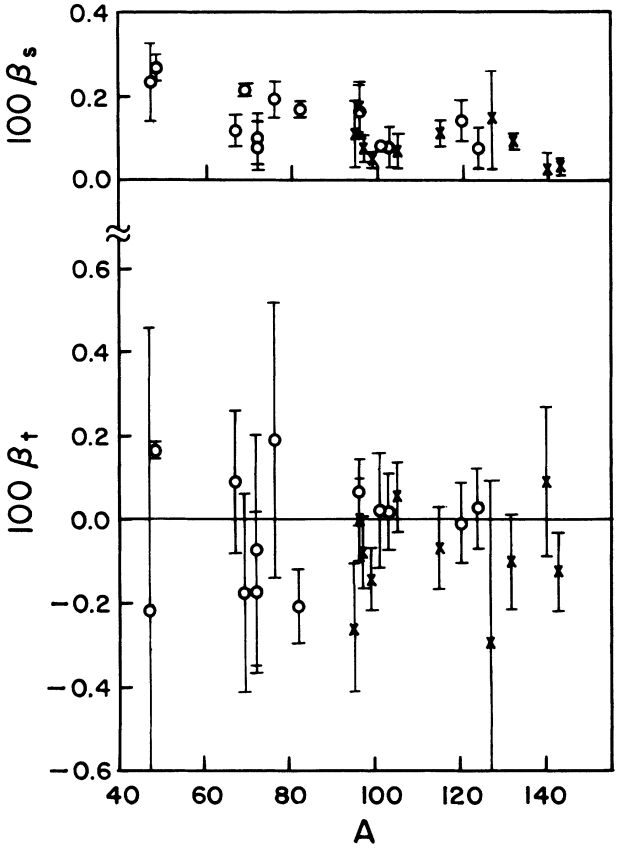

FIG. 11. Dependence of the parallel (β_s, top panel) and transverse (β_t, bottom panel) components of the source velocity on product mass for the fission/fragmentation component. ×, neutron-excessive fission products; ○, other products.

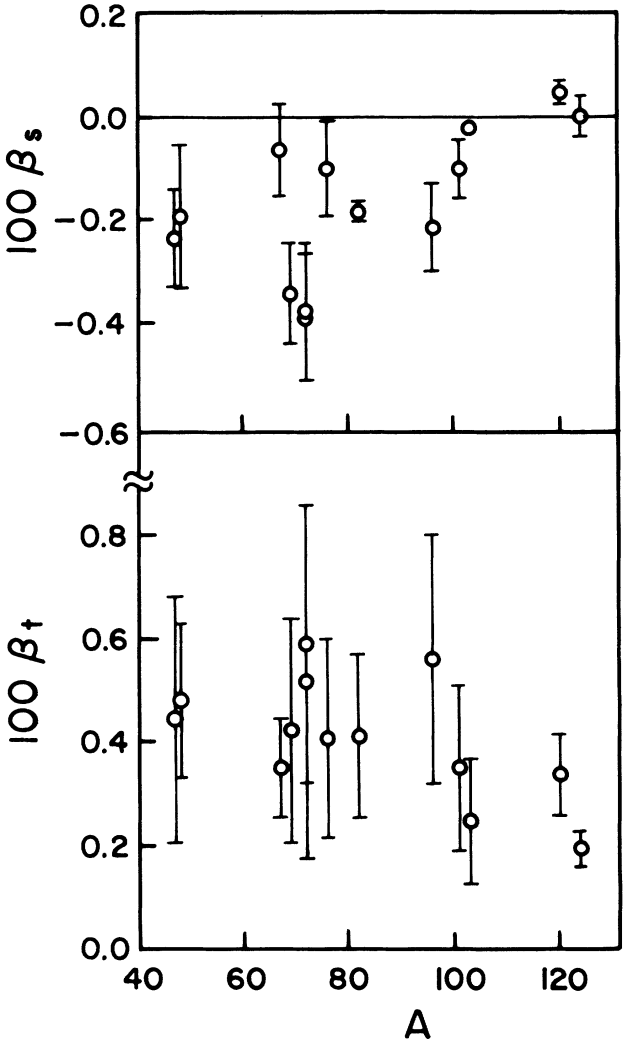

FIG. 12. Dependence of the parallel (β_s, top panel) and transverse (β_t, bottom panel) components of the source velocity on product mass for the deep spallation component.

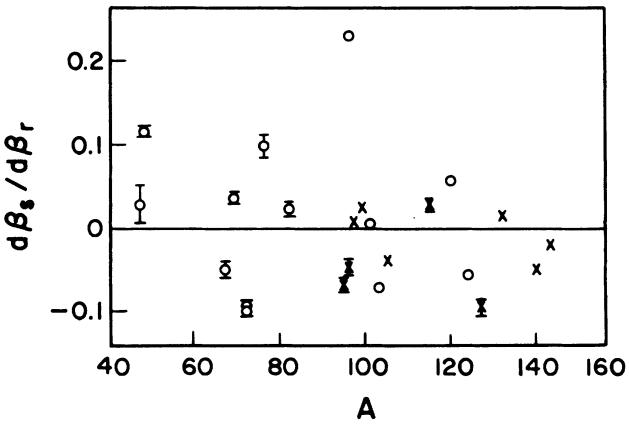

FIG. 13. Dependence of $d\beta_s/d\beta_r$ on product mass for the fission/fragmentation component. See Fig. 11 for details.

The results obtained for fission or fragmentation are generally consistent with the results of the thermal breakup model. Thus the values of β_s are essentially equal to the β values obtained in that analysis, albeit of lower accuracy. The values of β_t are consistent with zero for nearly all the products, as was assumed in Sec. IV A. This result suggests that the peak at sideward angles observed for these products reflects the intrinsic angular distribution rather than resulting from kinematic focusing towards these angles by the motion of the source. Figure 13 shows that the values of $d\beta_s/d\beta_r$ scatter about zero indicating that there is no significant correlation between source and fragment velocities.

The results for the deep spallation component are significantly different from those for the high-energy component. Figure 12 shows that the values of β_s are negative for all but the heaviest products. Furthermore,

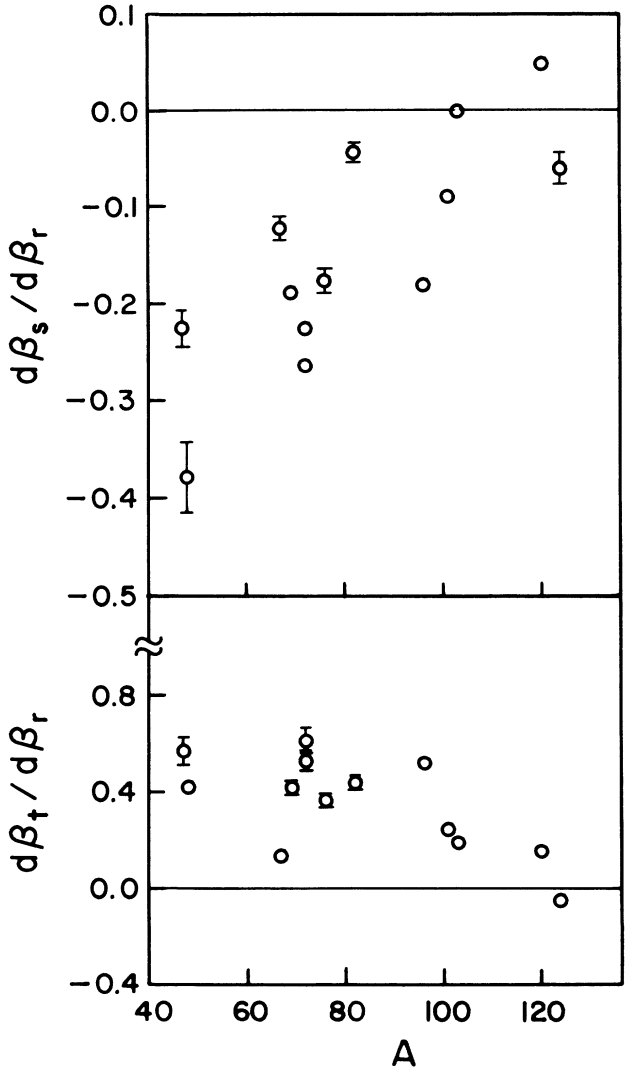

FIG. 14. Dependence of $d\beta_s/d\beta_r$ (top panel) and $d\beta_t/d\beta_r$ (bottom) for the deep spallation component.

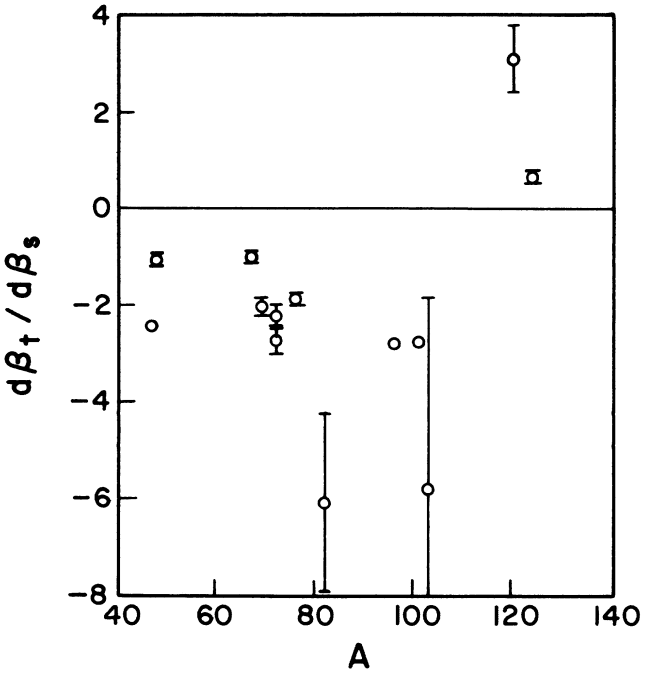

FIG. 15. Dependence of $d\beta_t/d\beta_s$ on product mass for the deep spallation component.

the values of β_t are significantly larger than zero. Taken together, these observations suggest that the deep spallation products are formed in the deexcitation of remnants moving at large angles to the beam. The results obtained for ^{47}Ca and ^{48}Sc, the lightest fragments observed in this work, are in line with those obtained for heavier products. It therefore appears that these products are formed both in deep spallation and in fragmentation, even though the spectra do not show the presence of two distinct components.

Figure 14 shows that the motion of the source of the deep spallation products is correlated with that of the products. The values of $d\beta_s/d\beta_r$ are negative for all but the heavier products. Since the values of β_s are negative, it follows that the source velocity increases in magnitude with the fragment velocity. A similar correlation is observed between the transverse component of the source velocity and the fragment velocity. Finally, Fig. 15 shows that, with the exception of the heaviest products, the values of $d\beta_t/d\beta_s$ are negative, indicating that the two components of the source velocity are correlated in magnitude. Evidently, the formation of these low-energy intermediate mass products does not involve two temporally well separated steps. Rather, the backward motion of the parent source is reflected in the motion of the products. This conclusion is consistent with that obtained in the preceding section.

D. Angular distribution as a function of fragment energy

The differential cross sections may be recast in the form of angular distributions of energy-selected fragments. Figure 16 shows the results for ^{69}Zn^m, which are

typical of all products in that the angular distributions evolve from backward peaked at low energies to forward peaked at high energies. As already noted, the low-energy deep spallation component has a more backward-enhanced angular distribution than the high-energy component. These results are certainly consistent with the more detailed angular distributions shown in Fig. 16. However, the latter indicate that the changes with energy are gradual and are not just associated with the change from deep spallation to fission or fragmentation.

Hüfner and Sommermann[8] have proposed a fast breakup model to explain the less complete angular distributions of energy-selected scandium fragments from 400 GeV proton interactions with uranium previously reported by our group.[5] Since our analysis shows that, with the exception of some of the fission products, the products of interest are not formed in a two-step process, comparison of the data with a fast breakup model is appropriate.

The Hüfner model assumes that the angular distribution is determined by the net effect of three factors: (1) an isotropic contribution from the Fermi motion in the remnant, (2) the sideward-to-forward directed momentum of captured spray particles resulting from the passage of the

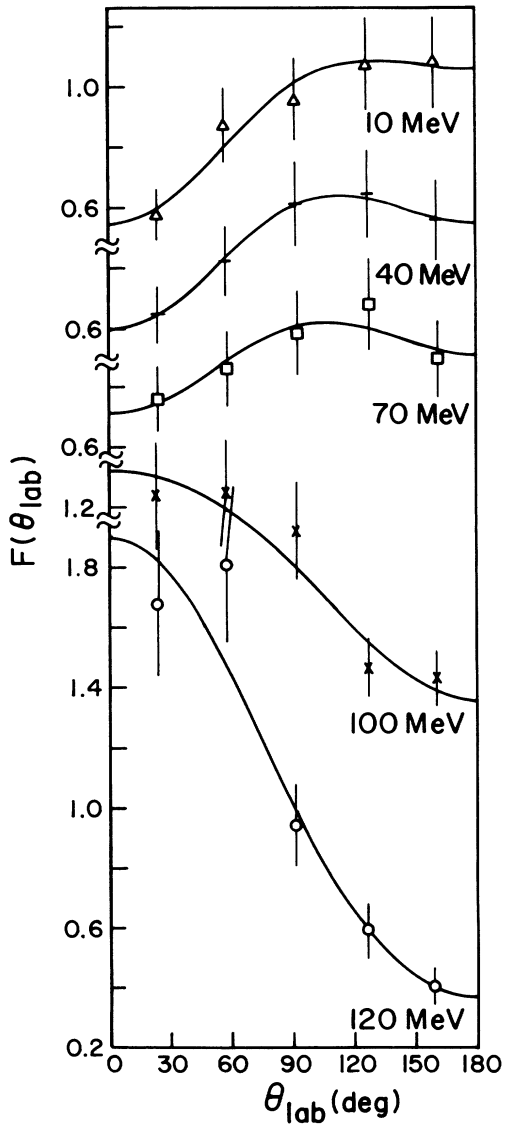

FIG. 16. Angular distribution of energy-selected ^{69}Zn^{m} fragments. The curves are fits of Eq. (1).

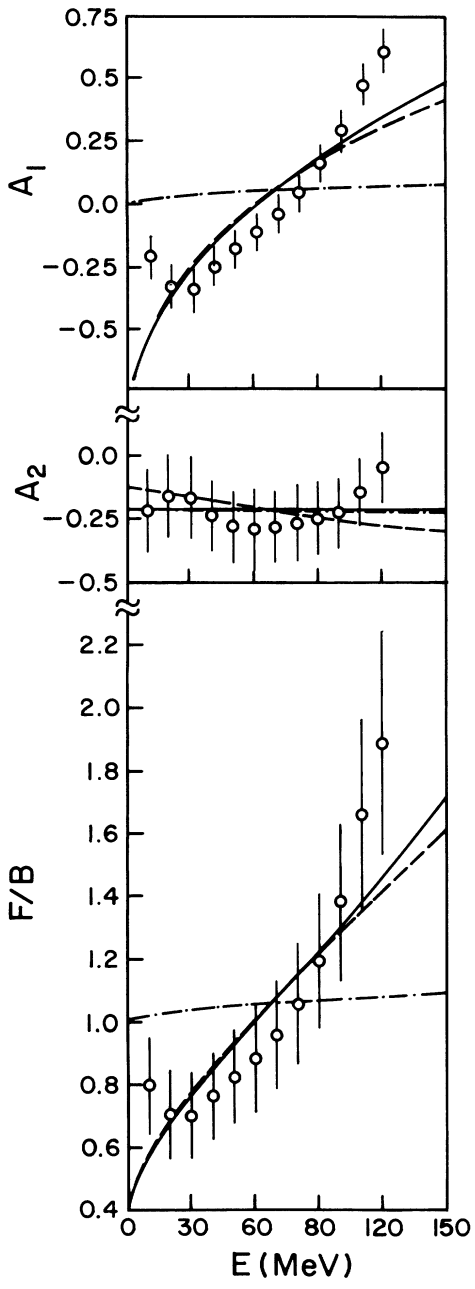

FIG. 17. Dependence on fragment energy of the angular distribution parameters A_1 and A_2 and of F/B for ^{48}Sc. The solid curves are a fit of the Hüfner model (Ref. 8) to the data points. Dashed curves, σ_q is constrained to $\geq 0.5\bar{q}_{\parallel}$; dot-dashed curves, χ is constrained to ≤ 0.

projectile, and (3) the sideward-to-backward directed momentum from Coulomb repulsion between the fragments. The double-differential cross sections are parametrized in terms of the following five quantities, which express the effect of the above factors: σ_F, the rms Fermi momentum; $\bar{q}_{\parallel}$, the mean forward component of momentum of spray particles and σ_q, the standard deviation of the momentum distribution; χ, the angle under which the Coulomb force acts on the prefragment (χ is measured backward from an axis perpendicular to the beam direction); and V_c, the magnitude of the Coulomb barrier. The values of these parameters are most conveniently obtained from the combined fit of the model to the energy dependence of the angular distribution coefficients A_1 and A_2 and to that of the forward-to-backward emission ratio F/B, obtained by integration of

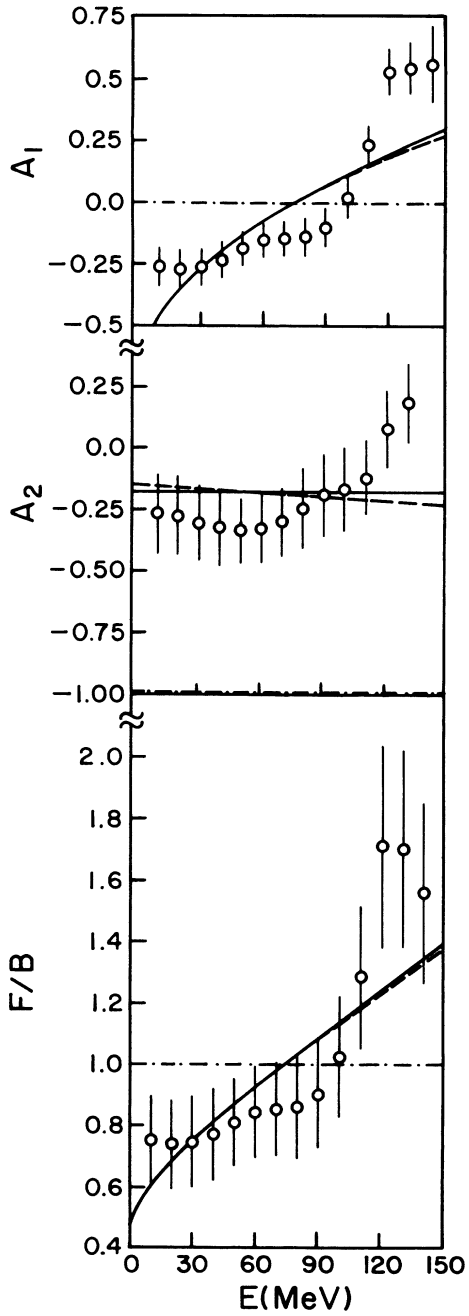

FIG. 18. Energy dependence of A_1, A_2, and F/B for ^{72}As. See Fig. 17 for details.

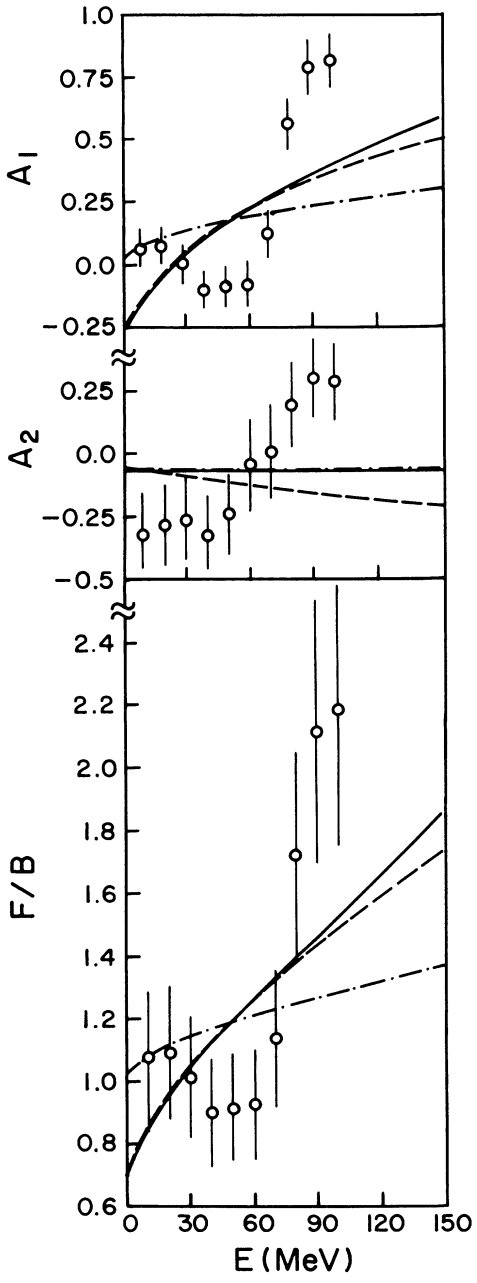

FIG. 19. Energy dependence of A_1, A_2, and F/B for ^{120}Sb^m. See Fig. 17 for details.

the angular distributions.

Figures 17–20 show some typical examples of these fits as performed with MINUIT. The values of A_1 and of F/B generally increase with energy, as expected from the evolution of the angular distributions depicted in Fig. 16. On the other hand, A_2 is relatively independent of energy. The fitted curves show a qualitatively similar behavior, although the fits are often rather poor.

Figures 21–25 show the variation with product mass of the parameters obtained from the fits to the data. The values of σ_F, Fig. 21, show the expected increase with fragment mass number and range from approximately 600 to 1500 MeV/c. The magnitude of these values is consistent with the Goldhaber formula.[34]

The spray particle parameters $\bar{q}_{\parallel}$ and σ_q are plotted in Figs. 22 and 23, respectively. The mean longitudinal momentum of the spray particles does not vary in a consistent way with mass number; the individual values range from $\sim$20 to 500 MeV/c, the mean value being $\sim$300 MeV/c. The mean value has a reasonable magnitude since it indicates that the initial proton-uranium interaction results in the capture of 2–6 spray particles.[8] The parameter σ_q is consistent with zero for virtually all products. This result is surprising since σ_q and $\bar{q}_{\parallel}$ are expected to have comparable values. However, the fits are rather insensitive to the value of σ_q. Thus Figs. 17–20 show the effect of setting σ_q equal to $0.5\bar{q}_{\parallel}$. Almost comparable agreement is obtained as when σ_q is allowed to vary freely.

The Coulomb barrier V_c, Fig. 24, generally lies in the range of 20–50 MeV, and appears to increase with fragment mass number. Coulomb energies generally are somewhat lower than the peak energies in fragment spectra. The values of V_c fulfill this criterion in most instances and are therefore reasonable.

The angle χ, shown in Fig. 25, fluctuates between approximately 15° and 50° and does not depend in a very systematic way on mass number. The values of χ are to a large extent inconsistent with the Hüfner model. According to this model, backward emission results from the trumpet-shaped geometry of the instability region created by the initial interaction. Only the light frag-

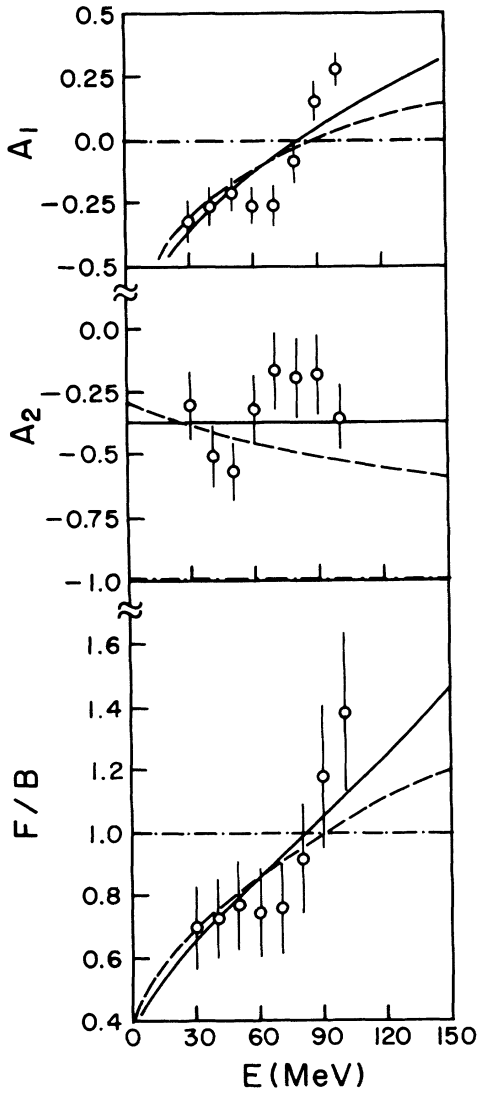

FIG. 20. Energy dependence of A_1, A_2, and F/B for ^{127}Sb. See Fig. 17 for details.

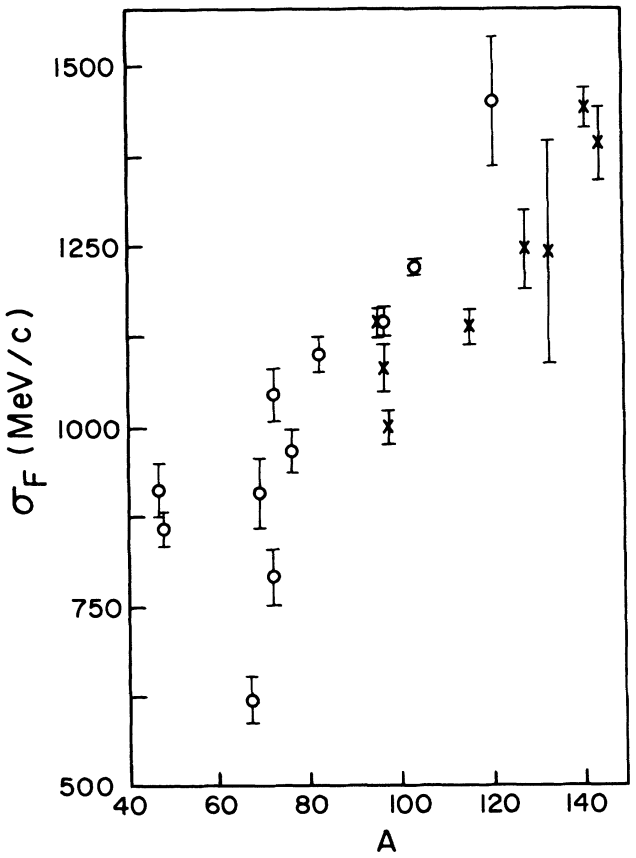

FIG. 21. Mass dependence of the parameter σ_F.

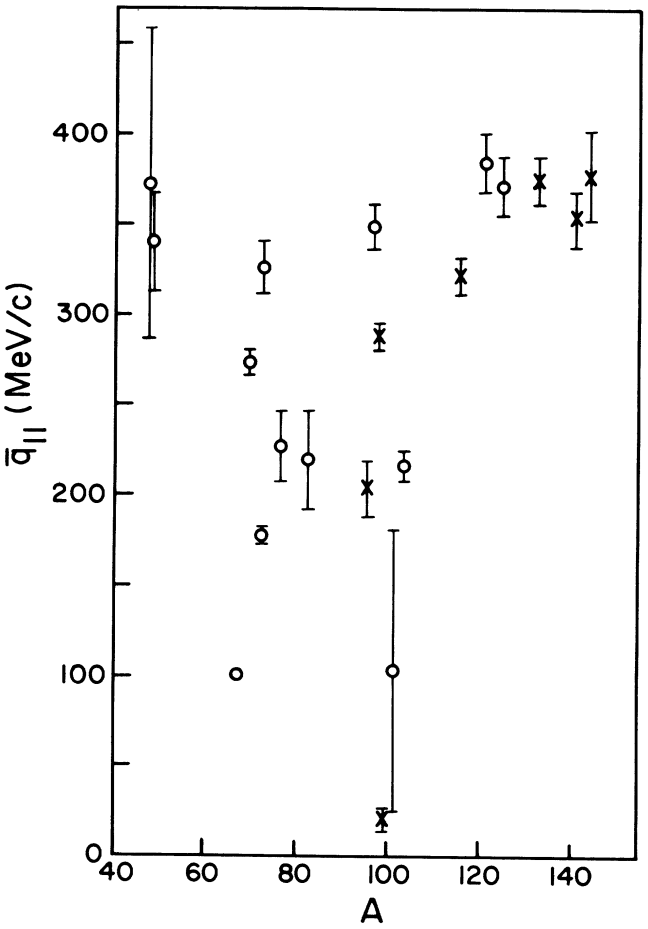

FIG. 22. Mass dependence of the parameter $\bar{q}_{\|}$.

ments can be propelled at backward angles (i.e., $\chi > 0$) by Coulomb repulsion, while the heavy fragments must be preferentially emitted at forward angles. However, Fig. 25 shows that even the heaviest observed fragments require rather large values of χ. Forcing χ to be ≤ 0 results in unacceptably poor fits to the data, as illustrated in Figs. 17–20.

If one demands that the parameters obtained from a fit of the Hüfner model be physically reasonable then the best agreement with the data is obtained for Sc frag-

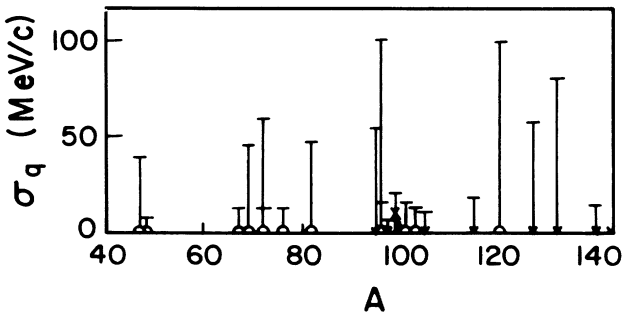

FIG. 23. Mass dependence of the parameter σ_q.

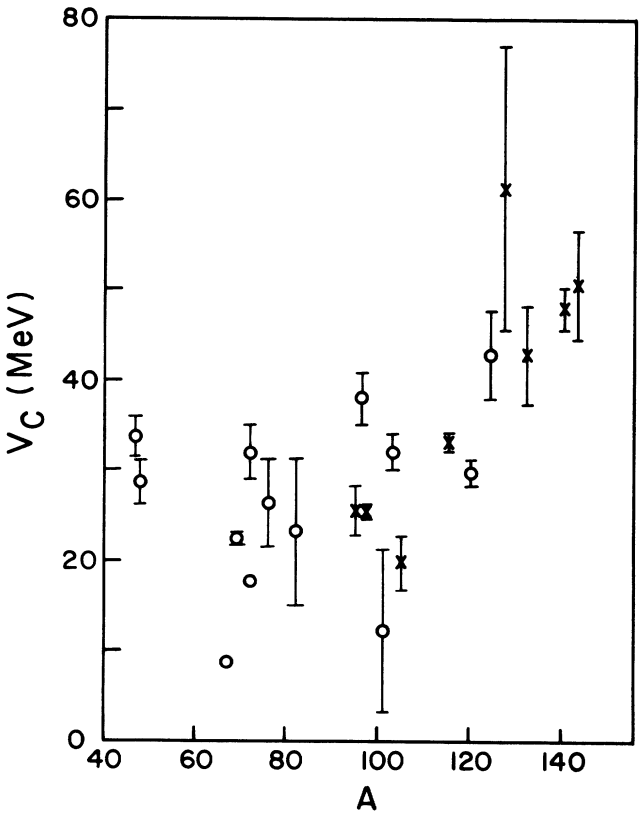

FIG. 24. Mass dependence of the parameter V_c.

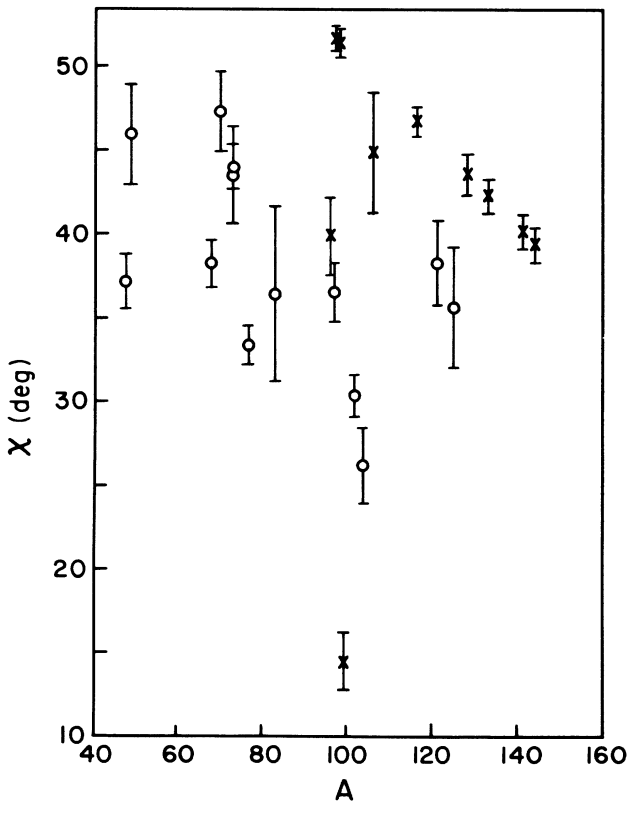

FIG. 25. Mass dependence of the parameter χ.

ments. Indeed, our earlier work on the emission of Sc fragments[5] provided the data that stimulated the development of this model. However, the more complete data presented here indicate that the model may have only limited applicability.

V. CONCLUSIONS

Energy spectra of 23 fragments, ranging from ^{47}Ca to ^{143}Ce, have been obtained from differential range measurements at five angles to the beam for the interaction of ^{238}U with 400 GeV protons. A thermal model fit has been used to decompose the spectra of intermediate mass fragments and neutron-deficient products in the fission product mass region into two components. The low-energy component increases in magnitude with decreasing energy, as expected for deep spallation. The high-energy component is Maxwellian-like in shape and consistent with fragmentation for the lighter products or with fission. The yield of the low-energy component is enhanced at backward angles relative to that of the high-energy component.

The results have been used to test the validity of the two-step model, have been subjected to an invariant cross-section analysis, and have been used to test the Hüfner fast breakup model. The analysis shows that the deep spallation products appear to be formed in the deexcitation of remnants moving at large angles to the beam and that the source and fragment velocities are correlated in magnitude. On the other hand, the fission and fragmentation products result from the breakup of remnants moving slowly along the beam direction. The velocity of these remnants appears to be uncorrelated with that of the fragments. While the formation of some of the fission products is consistent with a two-step model, this is not the case for any of the deep spallation or fragmentation products. However, even though these products appear to be formed in a fast breakup process, the variation of their angular distributions with energy is not, in most instances, accurately predicted by the Hüfner model.

ACKNOWLEDGMENTS

The cooperation of the Fermilab staff is gratefully acknowledged. We wish to thank Dr. T. C. Sangster for his help with the code MINUIT and Dr. H. M. Sommermann for discussions concerning the Hüfner model. This work was supported by the U. S. Department of Energy.

[1]J. B. Cumming, R. J. Cross, J. Hudis, and A. M. Poskanzer, Phys. Rev. **134**, B167 (1964).
[2]V. P. Crespo, J. B. Cumming, and A. M. Poskanzer, Phys. Rev. **174**, 1455 (1968).
[3]V. P. Crespo, J. B. Cumming, and J. M. Alexander, Phys. Rev. C **2**, 1777 (1970).
[4]J. A. Urbon, S. B. Kaufman, D. J. Henderson, and E. P. Steinberg, Phys. Rev. C **21**, 1048 (1980).
[5]D. R. Fortney and N. T. Porile, Phys. Rev. C **22**, 670 (1980).
[6]A. M. Poskanzer, G. W. Butler, and E. K. Hyde, Phys. Rev. C **3**, 882 (1971).
[7]G. D. Westfall, R. G. Sextro, A. M. Poskanzer, A. M. Zebelman, G. W. Butler, and E. K. Hyde, Phys. Rev. C **17**, 1368 (1978).
[8]J. Hüfner and H. M. Sommermann, Phys. Rev. C **27**, 2090 (1983).
[9]D. L. Klingensmith and N. T. Porile, Phys. Rev. C **36**, 1051 (1987).
[10]T. Routti and S. G. Prussin, Nucl. Instrum. Methods **72**, 125 (1969).
[11]D. R. Fortney and N. T. Porile, Phys. Rev. C **21**, 664 (1980).
[12]D. R. Fortney and N. T. Porile, Phys. Rev. C **21**, 2511 (1980).
[13]C. R. Rudy, N. T. Porile, and S. B. Kaufman, Nucl. Instrum. Methods **138**, 19 (1976).
[14]D. L. Klingensmith, Ph.D. thesis, Purdue University, 1988 (unpublished).
[15]L. C. Northcliffe and R. F. Schilling, Nucl. Data Sec. A **7**, 233 (1970).
[16]J. Lindhard, M. Scharff, and M. E. Shiøtt, Kgl. Danske Videnskab. Selskab. Mat.-Fys. Medd. **33**, No. 14 (1963).
[17]J. B. Cumming (private communication).
[18]G. D. Cole and N. T. Porile, Phys. Rev. C **24**, 2038 (1981).
[19]Y. Y. Chu, G. Friedlander, and L. Husain, Phys. Rev. C **15**, 352 (1977).
[20]Ø. Scheidemann and N. T. Porile, Phys. Rev. C **14**, 1534 (1976).
[21]Y. W. Yu, S. Biswas, and N. T. Porile, Phys. Rev. C **11**, 2111 (1975).
[22]Y. W. Yu and N. T. Porile, Phys. Rev. C **10**, 167 (1974).
[23]Y. Y. Chu, E. M. Franz, G. Friedlander, and P. J. Karol, Phys. Rev. C **4**, 2202 (1971).
[24]J. A. Panontin and N. T. Porile, J. Inorg. Nucl. Chem. **32**, 1775 (1970).
[25]N. T. Porile, Phys. Rev. **148**, 1235 (1966).
[26]Y. W. Yu, Phys. Rev. C **22**, 933 (1980).
[27]N. T. Porile, D. R. Fortney, S. Pandian, R. A. Johns, T. Kaiser, K. Wielgoz, T. Chang, N. Sugarman, J. A. Urbon, D. J. Henderson, S. B. Kaufman, and E. P. Steinberg, Phys. Rev. Lett. **43**, 918 (1979).
[28]A. S. Hirsch, A. Bujak, J. E. Finn, L. J. Gutay, R. W. Minich, N. T. Porile, R. P. Scharenberg, B. C. Stringfellow, and F. Turkot, Phys. Rev. C **29**, 508 (1984).
[29]Computer Program Library, CERN, Geneva.
[30]K. Beg and N. T. Porile, Phys. Rev. C **3**, 1631 (1971).
[31]K. Nakai *et al.*, Phys. Lett. B **121**, 373 (1983).
[32]J. Gosset *et al.*, Phys. Rev. C **16**, 629 (1977).
[33]R. E. L. Green, R. G. Korteling, and K. P. Jackson, Phys. Rev. C **29**, 1806 (1984).
[34]A. S. Goldhaber, Phys. Lett. B **53**, 306 (1974).